Geoinformatics & Geostatistics: An Overview

Research Article

A SCITECHNOL JOURNAL

Geochemistry and Uranium Mineralization in Neoproterozoic Leucogranite of Gabal Homra Dom, South Eastern Desert, Egypt

Gehad M Saleh[1]*, Ibrahim H Ibrahim[1], Ibrahim A Salem[2] and Ibrahim B Abdel Kader[1]

[1]Nuclear Materials Authority, P.O. Box: 530 EL-Maadi, Cairo, Egypt.

[2]Faculty of science, Tanta University, Tanta, Egypt.

Abstract

Gabal (G.) Homra Dom leucogranite crops out about 65 km south of Shalatin City, South Eastern Desert of Egypt. It is an elongated mass extending NNW-SSE, bounded by two major sinstral strike slip faults and mainly composed of monzogranite. They intrude amphibolites, metavolcanics and volcano-sedimentary associations. The southern eastern contact between G. Homra Dom leucogranite and the volcano-sedimentary association is marked by a narrow sheared zone up to 5 m width. The sheared leucogranite samples are enriched with MgO, Na_2O, K_2O, Rb, Sr, Zr, Ba, V, Co in addition to Th and U and depleted in Al_2O_3 if compared with the average of the fresh leucogranite.

G. Homra Dom leucogranite exhibit calc-alkaline affinity and peraluminous to metaluminous compositions and could be generated by fractional crystallization of a granitic magma in late- to post collision granites. These are produced by circulation of fluids and alkali loss by vapor-phase transfer during late magmatic stage. The higher temperatures of the apatite model (950–1080°C) probably represent the initial temperature of the melt, whereas the lower temperature estimates from zircon suggests that these leucogranite was initially undersaturated with respect to zircon and hence the calculated temperature would not closely resemble original magmatic temperatures. The Homra Dom leucogranite were formed by partial melting of metagraywackes that are found in deeper part of the crust of the Arabian Nubian Shield.

The relationship between eU versus eTh and eU/eTh ratio versus eTh and eU reflect strong positive relation along sheared leucogranite which means that eU/eTh ratio tends to increase with uranium mobilization and post magmatic redistribution. The minerals cassiterite, molybdenite and wolframite with the secondary uranium minerals (uranophane) are identified by Environmental Scanning Electron Microscope (ESEM) and XRD. These minerals are formed at the end of magmatic stage, where the mineralized fluids enriched with Bi, W, Sn, Mo and F rises as post magmatic hydrothermal episode along the south eastern contact.

Keywords

Gabal Homra Dom; Leucogranite; Geochemistry; Peraluminous; Uranophane

***Corresponding author:** Gehad M Saleh, Nuclear Materials Authority, PO Box 530 EL, Maadi, Cairo, Egypt, E-mail: drgehad_m@yahoo.com

Received: July 16, 2019 **Accepted:** October 03, 2019 **Published:** November 06, 2019

Introduction

In Egypt, granitoids constitute about 50% of the basement complex. Two main granite types are distinguished, i.e. older and younger granitoids. The older group includes syn- to late- orogenic calc-alkaline rocks with compositions ranging from quartz diorite and tonalite to trondhjemite, granodiorite and sparse granite. They have been assigned ages of between 655 and 570 Ma [1] and make up about 27% of the basement in the Eastern Desert. The younger granitoid rocks are late- to post-orogenic and are suggested to have been intruded from about 570 Ma to about 500 Ma [2,3].

The younger granites are highly fractionated calc-alkaline to mildly alkaline rocks with an I-type affinity; some of them have been classified as A-type [4]. This group of granites includes a suite of peraluminous leucocratic granites characterized by compositions close to Ab–Or–Qz minimum melts in the H_2O-saturated haplogranite system as well as high modal muscovite and the presence of almandine–spessartine garnet [5,6]. Although strongly peraluminous leucogranites are of limited distribution in the Egyptian Shield, their close spatial association with gneisses and migmatites is important. They may be used to relate high-grade metamorphism and magmatism with tectono-metamorphic events in the Eastern Desert of Egypt.

The present study mainly deals with the geology, geochemistry, REEs of fresh and sheared leucogranite and briefly characterizes their petrography and mineralogy characteristics with emphasis on the uranium mineralization of G. Homra Dom leucogranite, South Eastern Desert, Egypt.

Geologic Setting and Petrography

G. Homra Dom area crop out at about 65 km south of Shalatin city. It is bounded by latitudes 22° 34´ and 22° 42´ N and longitudes 35° 35´ and 35° 42´ E (Figure 1). It is dominantly covered by amphibolite, metavolcanic and volcano-sedimentary association intruded by leucogranite. All rocks dissected by basic dykes and quartz veins.

The amphibolites are exposed along the western part of the mapped area (Figure 1). It is of low relief, green to dark grey colours and highly weathered, jointed, exfoliated. Some amphibolite xenoliths are recorded within the leucogranite rocks. The metavolcanics are exposed at the extreme south eastern part of the mapped area and are characterized by being highly tectonized, banded and foliated with steeply dip to E direction. The volcano-sedimentary rocks are associated with metavolcanic with inferred contact and occurs as a roof pended over G. Homra Dom leucogranite (Figure 2a). They are characterized by being highly tectonized, highly jointed in various directions and generally foliated NE-SW and dip 45° to SE direction.

The leucogranite of G. Homra Dom are characterized by low to moderate topography and cover about 25 km². They form elongated mass in NNW-SSE direction with about 2 km in width and 12 km. in length (Figure 1). They are pink to buff in colour while near the southern contact they are highly reddish in colour due to the hematitization. G. Homra Dom leucogranite is essentially roughly parallel to the regional foliation of the surrounding country rocks. Such a foliation not only decreases with the increase lateral distance from the contact but also it markedly differs in intensity according to the adjacent rock. The contact between the younger leucogranite and the volcano-sedimentary association is of sharp nature (Figure 2b) and marked by a narrow thermal and tectonized zone up to 3-5 m thick [7]. G. Homra Dom leucogranite is highly sheared due to bounded by two major sinstral strike slip faults and also dissected by numerous of NE-SW dextral and NW-SE sinstral faults. Where are there may contain some angular xenoliths from volcano-sedimentary rocks (Figure 2c) and send apophyses into the volcano-sedimentary association. They are also characterized by exfoliations, taffoni weathering structure and fractures filled with quartz veinlets (Figure 2d).

Petrography of the fresh leucogranite

Thirteen (13) fresh samples of G. Homra leucogranite were subjected to modal analysis for computing the volumetric percentages of their mineral assemblage (Table 1) and for the proper identification and nomenclature using Q-A-P diagram after [8]. The fresh granitic samples fall within the monzogranite field (Figure 3). They are medium- to coarse-grained and mainly composed of potash feldspars (36 in vol. %), quartz (30 in vol. %), plagioclase (28 in vol. %) and biotite (3.5 in vol. %), whereas muscovite, chlorite and sericite are alteration products. Garnet, allanite, zircon, titanite, cassiterite, apatite, epidote and opaques are accessories (2.5 in vol. %). The rocks exhibit equigranular and micrographic textures.

Potash feldspars occur as subhedral perthite and microcline perthite crystals (Figure 4a) with patchy, string and braided types. They poikilitically enclose quartz, small plagioclase laths, biotite, minute crystals of muscovite and opaques. Quartz occurs as anhedral crystals with irregular boundaries and sometimes intergrown with potash-feldspars forming micrographic texture (Figure 4b). Plagioclase (An 6-17) forms subhedral tabular crystals and exhibit albite, combined and Carlsbad twinning (Figure 4c). Small plagioclase laths with albite lamellar growth at the outer rims around perthite crystals. Biotite forms subhedral kinked flakey crystals (Figure 4d) with pleochroic as: X= yellowish brown, Y= brown and Z= dark brown and greenish brown. It is partly altered to chlorite and iron oxides and encloses quartz, fluorite and small plagioclase laths. Garnet, allanite, cassiterite, zircon and titanite are accessories. Garnet is yellowish brown to reddish orange in colour (Figure 4e). Allanite is brown colour and pleochroic from pale brown to dark brown (Figure 4f). Cassiterite is a brown reddish black in colour (Figure 4g). Titanite is characterized by sphenoidal shape (Figure 4h).

Petrography of the sheared leucogranite

The sheared leucogranite (Figure 5a) locates at the southeastern part of G. Homra Dom and constitutes an elongated mass with about 300 m length and 170 m width sharp contact with the volcano-sedimentary association (Table 1). The rocks are highly weathered, fractured and mainly composed of quartz, potash feldspar, plagioclase, biotite.

The alteration impacts on the essential minerals of these sheared rocks are as follows: (1) Quartz shows strong undulose extinction and

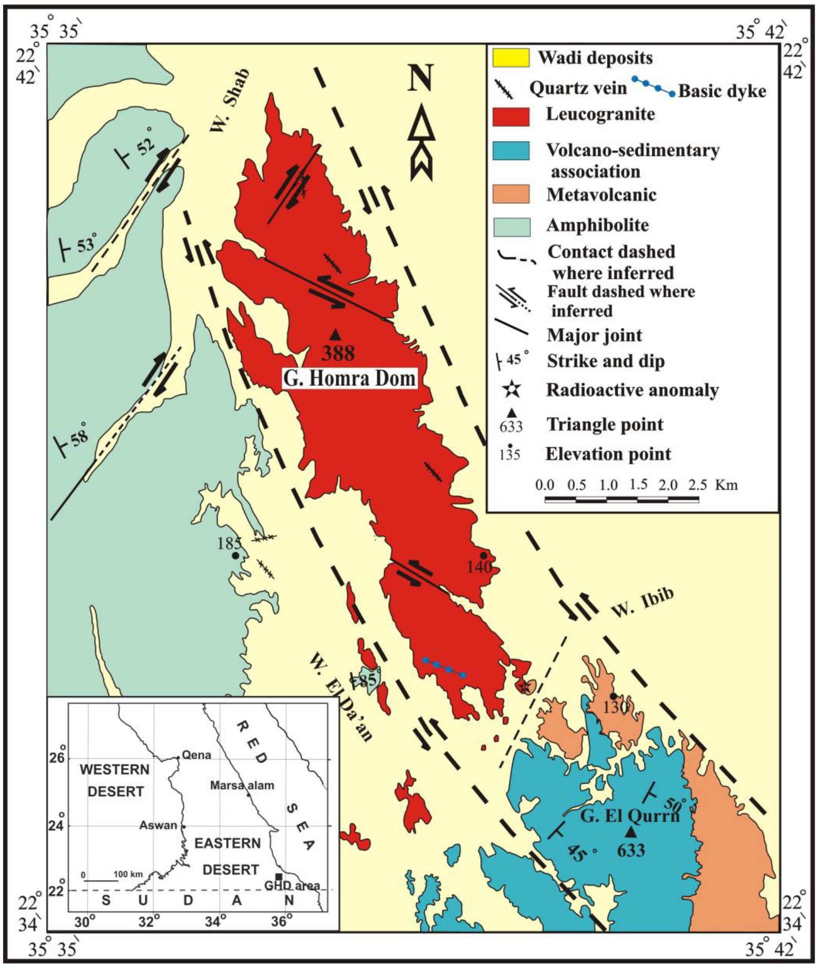

Figure 1: Geologic map of G. Homra Dom Area, South Eastern Desert, Egypt.

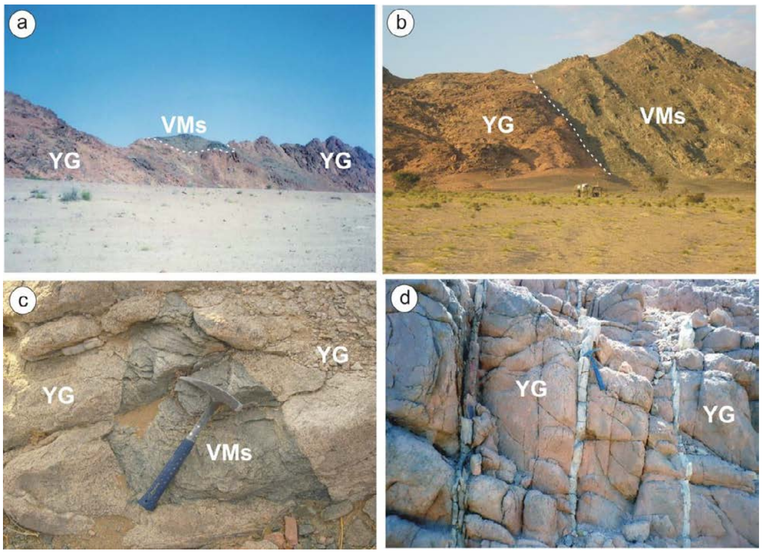

Figure 2: (a) Volcano-sedimentary association (VMs) as a roof pendant on late tectonic younger (YG), looking N., (b) Sharp contact between the volcano-sedimentary association (VMs) and younger leucogranite (YG), looking E., (c) Angular xenolith from of volcano-sedimentary association in younger leucogranite, looking E. and (d) Quartz veins filling the fractures in younger leucogranite, looking E.

Table 1: Modal composition of the fresh leucogranite samples.

S. No.	Qz	Plag.	K-feld.	Bio.	Op.	Acc.	Q	P	A
H-4	30.5	38.8	25.9	3.2	1.4	0.2	32	40.8	27.2
H-5	25.9	27.6	41.4	2.5	2.6	-	27.3	29.1	43.6
H-6	24	31.3	38.1	4	2	0.6	25.7	33.5	40.8
H-8	32.5	39.2	23.9	3.5	0.5	0.4	34	41	25
H-9	25	38.5	31.5	3	1.6	0.4	26.3	40.5	33.2
H-11	32	25	37.5	3	2	0.5	33.86	26.46	39.68
H-12	22	31.5	43.4	1.9	0.4	0.8	22.7	32.5	44.8
H-13	28.9	41.7	24.6	3.3	1.2	0.3	30.4	43.8	25.8
H-14	21	42.8	35	0.8	-	0.4	21.3	43.3	35.4
H-15	34.9	32.1	26.3	4.8	1.2	0.7	37.4	34.4	28.2
H-16	40.2	21.5	32	3.6	2.1	0.6	42.9	22.9	34.2
H-17	30.5	24.7	36.9	4.5	2	1.4	33.1	26.8	40.1
H-23	33	18.6	43.3	3.1	1.4	0.6	34.8	19.6	45.6
Average	**29.26**	**31.79**	**33.83**	**3.17**	**1.53**	**0.58**	**30.9**	**33.44**	**35.66**

Note: S. No.=sample number, Qz=quartz, Plag.=plagioclase, K-feld.=potash feldspar including perthite, Bio.=biotite, Acc.=accessory and Op.=opaques. Q=quartz content, P=plagioclase content and A=potash feldspar content. (All values are in volume percent).

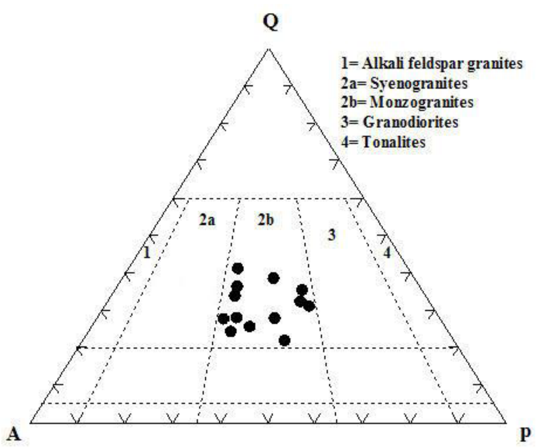

Figure 3: Modal analyses of the fresh leucogranite samples, G. Homra Dom, after [8].

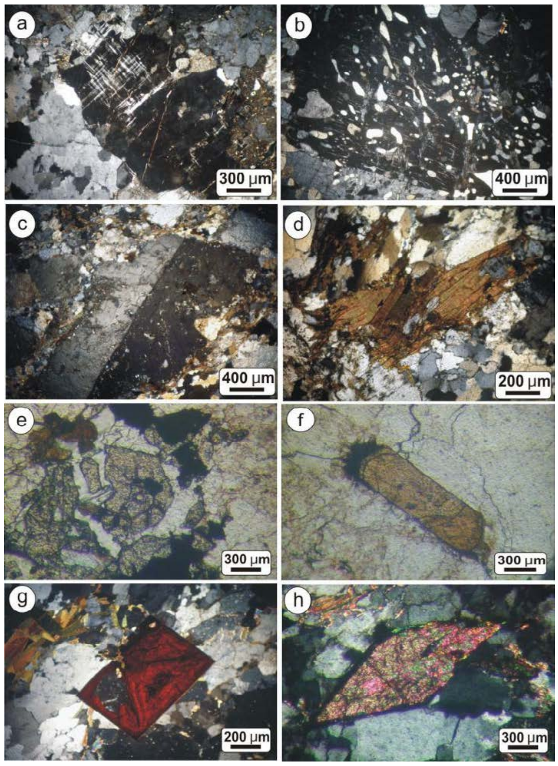

Figure 4: (a) Cross hatching in microcline crystal, (b) Micrographic texture, (c) Carlsbad twinning in plagioclase crystal and corroded by quartz, (d) Biotite flakes corroded by secondary quartz, (e) Euhedral garnet crystal under P.P., (f) Euhedral allanite with zonal structure under P.P., (g) Zoning in euhedral cassiterite crystal, and (h) Euhedral titanite crystal, showing wedge shape, Homra Dom leucogranite, SED, Egypt.

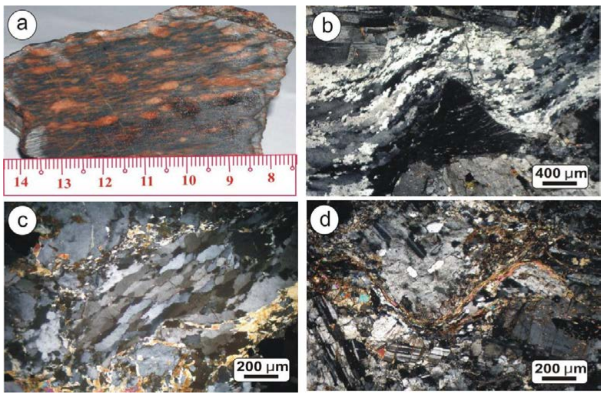

Figure 5: (a) Mylonitization in polished slab, (b) Bending fussy quartz due to stress effect, (c) S-shape microfolding biotite flakes, and (d) Banded biotite and quartz, Homra Dom sheared leucogranite, SED, Egypt.

fussy structure (Figure 5b). (2) Secondary quartz interstices show banding which indicates the recrystallization process (Figure 5c). (3) Potash-feldspars (perthites) are often stained with iron oxides and small plagioclase laths over-grow between the patchy perthite crystals. (4) Plagioclases occur as cloudy crystals due to moderate alteration and others plagioclase crystals are cracked and filled by iron oxides and quartz veinlets. (5) Deformed plagioclases are observed as dislocated lamellae. (6) Some plagioclase crystals extrude quartz as worms in the crystals producing myrmekitic texture and other crystals show zonation with alteration to muscovite and sericite. (7) Biotite show bending and forming S-shaped crystals (Figure 5d). (8) Fluorite veinlets are seen associated the other accessories and opaques.

Geochemistry of the Leucogranite

Analytical methods

Chemical analyses were performed for thirty (30) selected samples (19 fresh and 11 sheared) from G. Homra Dom. Nineteen fresh leucogranite samples were analyzed at the laboratories of the Polish Geological Institute, Warszawa, Poland. The major elements are determined on fused pellets prepared according to the method of [9] using lithium tetraborate as a flux. Some trace elements are determined on pressed powder pellets. The REE_S, Sc, Hf, Ta, Th and U are analyzed using instrumental neutron activation analysis (INAA). The accuracy and precision of the analytical results were found to be in the range 1-3% for the major elements, 10-15% for the trace elements and 5-10% for the Hf, Th, U and REEs. Eleven (11) sheared leucogranite samples were analyzed at the laboratories in Kyushu Univ., Japan. The major oxides were determined by wet chemical technique method [10]. The significant trace elements are determined by X-ray fluorescence method (Philips-PW 1480 X-ray spectrometer X- unique II with automatic sample changer PW 1510).

Major and trace elements geochemistry of the fresh leucogranite

The results of the whole rock analyses are given in Table 2. The Normative Q*-ANOR classification diagram after [11], where $Q^*=100Q/(Q+Or+Ab+An)$ and $ANOR=100An/(Or+An)$. The data fall in monzogranite field (Figure 6a). The binary relation $1000 (MgO+FeO^*+TiO_2)/SiO_2$ versus $(Al_2O_3+CaO)/(FeO^*+Na_2O+K_2O)$ has been used by [12] to distinguish between calc-alkaline, alkaline and highly fractionated calc-alkaline granites. In this diagram (Figure 6b) the investigated samples plot in the fields of highly fractionated calc-alkaline and peraluminous calc-alkaline granites. Calculation of the Shand Index according to [13] for the examined granitoids indicates that the G. Homra Dom granitic rocks are mainly peraluminous nature except one sample fall in metaluminous field (Figure 6c). On the basis of the tectonomagmatic discrimination diagrams of [14], the G. Homra Dom leucogranite can be classified to late tectonic granites due to the sample fall in lat- to post-collision granites (LP-CLOG) field (Figure 6d).

Rb, Sr and Ba are the most useful trace elements to evaluate the fractional crystallization model in granitoids because their behaviour in these rocks is strongly related to the major minerals such as feldspar and Bucanan [15] suggested that the higher Rb/Sr ratio (>1.5) is pre-existing felsic material in the source region, but Rb/Sr of low range (<0.7) suggests derivation from upper mantle. The average of G. Homra Dom leucogranite samples give Rb/Sr ratio=0.9 on diagram after [16] (Figure 6e) that display as depletion of Sr due to crystallization of feldspars. As this plot shows the same trend for all members of the petrogenitic sequence, they could be produced by a single process. The Ba–Rb diagram of [17] show that G. Homra Dom leucogranite samples are plot around line 4.4 × 10 (Figure 6f). The ratio of Ba/Rb decreases with increasing differentiation due to crystallization of the feldspars (Figure 6g). The average crustal ratio of Ba/Rb for the studied leucogranite (Ba/Rb=3.8) nearly similar that of normal granite of about 4 [18].

Petrogenetic implications

Magmatic temperatures of the studied samples can be obtained from the apatite and zircon saturation estimates [19]. These estimates are based on models of the temperature of apatite and zircon

Table 2: Major (wt%), trace (ppm) and REEs of the fresh leucogranite, G. Homra Dom, SED, Egypt.

	1	**2**	**3**	**4**	**5**	**6**	**7**	**8**	**9**	**10**	**11**	**12**	**13**	**14**	**15**	**16**	**17**	**18**	**19**	**Av.**
SiO_2	72.73	73.44	72.45	73.61	73.36	71.97	74.54	73.58	75.34	75.36	73.51	72.95	74.96	75.53	75.12	75.77	74.69	74.7	73.14	**74.04**
TiO_2	0.23	0.21	0.22	0.23	0.25	0.22	0.21	0.23	0.19	0.22	0.21	0.21	0.13	0.14	0.16	0.19	0.21	0.23	0.21	**0.21**
Al_2O_3	14.65	13.94	13.75	13.84	13.89	12.92	13.62	13.62	13.46	13.51	13.52	13.63	13.12	13.06	13.87	13.11	13.61	13.03	13.51	**13.56**
Fe_2O_3	1.82	1.85	1.74	1.71	1.9	1.65	1.7	1.89	1.58	1.66	1.83	1.55	1.56	1.42	1.47	1.15	1.3	1.57	1.49	**1.62**
MnO	0.08	0.07	0.07	0.06	0.07	0.07	0.08	0.08	0.07	0.06	0.08	0.06	0.03	0.02	0.04	0.05	0.03	0.08	0.09	**0.06**
MgO	0.34	0.31	0.27	0.26	0.35	0.34	0.28	0.29	0.27	0.31	0.29	0.86	0.05	0.06	0.14	0.19	0.12	0.35	0.34	**0.29**
CaO	1.7	1.45	1.41	1.31	1.32	1.08	1.28	1.47	1.09	1.08	1.29	1.07	0.69	0.59	0.61	0.67	0.72	1.02	1.73	**1.14**
Na_2O	4.54	3.62	3.65	3.44	3.49	3.34	3.54	3.61	3.56	3.5	3.65	3.38	3.86	3.78	3.79	3.89	3.71	3.54	3.29	**3.64**
K_2O	3.32	4.55	4.39	4.16	4.62	4.5	4.43	4.14	4.38	4.24	4.19	4.21	4.52	4.43	4.42	4.45	4.32	4.38	4.44	**4.32**
P_2O_5	0.07	0.08	0.08	0.07	0.09	0.09	0.08	0.09	0.08	0.09	0.07	0.08	0.03	0.02	0.03	0.04	0.05	0.09	0.14	**0.07**
L.O.I.	0.79	0.84	1.5	0.94	0.87	1.41	0.66	0.89	0.71	0.79	1.19	1.29	0.57	0.43	0.38	0.41	0.42	0.76	0.96	**0.83**
Total	**100.27**	**100.36**	**99.53**	**99.63**	**100.21**	**97.59**	**100.42**	**99.89**	**100.73**	**100.82**	**99.83**	**99.29**	**99.52**	**99.48**	**100.03**	**99.92**	**99.18**	**99.75**	**99.34**	**99.78**
Rb	143	149	138	140	142	132	134	137	131	139	128	142	109	111	115	130	117	116	120	**130**
Sr	139	135	145	139	143	144	141	143	126	136	145	128	165	150	149	136	121	122	118	**138**
Y	23	25	23	24	24	21	22	21	19	24	20	23	14	16	20	21	20	34	27	**22**
Zr	164	166	175	171	176	162	160	169	147	165	156	160	145	82	78	80	70	144	141	**143**
Nb	15	12	11	13	12	13	11	12	10	13	12	13	10	12	16	15	16	15	12	**13**
Ba	532	475	548	482	575	552	457	475	460	483	564	481	486	488	516	458	339	432	337	**481**
V	10	11	7	9	10	8	10	11	6	8	10	7	4	7	8	10	7	7	9	**8**
Cr	23	27	25	21	25	24	27	25	32	18	35	21	22	20	22	21	19	28	31	**25**
Co	2	2	3	2	2	3	3	3	2	2	2	2	2	3	2	2	2	3	2	**2**
Ni	8	9	10	9	10	9	11	8	10	12	9	10	7	8	9	7	6	10	3	**9**
Hf	4.8	4.2	4.4	4.7	4.9	4.1	5.2	4.3	5.1	5.4	3.7	4.2	3.2	3.9	4.3	4	4.6	4.1	4.5	**4**
Ga	10	12	14	10	11	13	14	16	15	13	12	10	10	11	10	10	13	14	10	**12**
Qz	29.83	31.78	31.85	35.14	32.49	34.05	34.14	33.74	35.35	36.24	33.71	34.51	34.12	35.65	34.87	34.69	35.45	35.24	33.72	**34.03**
Or	19.74	27.04	26.49	24.93	27.51	27.67	26.27	24.74	25.9	25.07	25.13	25.41	27.02	26.45	26.24	26.45	25.87	26.17	26.69	**25.83**
Ab	38.57	30.74	31.47	29.46	29.69	29.35	29.99	30.82	30.08	29.57	31.27	29.15	32.97	32.25	32.14	33.04	31.75	30.22	28.26	**31.09**
An	8.07	6.76	6.66	6.17	6.06	5.02	5.9	6.84	4.94	4.83	6.08	4.94	3.28	2.84	2.86	3.11	3.32	4.58	7.89	**5.27**
C	0.64	0.58	0.6	1.45	0.93	0.8	0.83	0.71	1.04	1.38	0.78	1.76	0.68	1.01	1.8	0.75	1.64	0.8	0.44	**0.98**
Hy	0.85	0.78	0.69	0.66	0.88	0.88	0.7	0.73	0.67	0.77	0.73	2.19	0.13	0.15	0.35	0.48	0.3	0.88	0.86	**0.72**
Mt	0.26	0.23	0.23	0.2	0.23	0.24	0.26	0.26	0.23	0.2	0.27	0.2	0.1	0.07	0.13	0.16	0.1	0.26	0.3	**0.21**
He	1.65	1.7	1.61	1.6	1.75	1.55	1.73	1.73	1.42	1.52	1.67	1.44	1.51	1.39	1.38	1.04	1.25	1.4	1.31	**1.51**
Ap	0.15	0.18	0.18	0.15	0.2	0.2	0.2	0.2	0.17	0.2	0.15	0.18	0.07	0.04	0.07	0.09	0.11	0.2	0.31	**0.16**

Fe_2O_3 is total iron

saturation using P_2O_5 and Zr concentration in the granites (Figures 7a&b). The higher temperatures of the apatite model (950-1080°C) probably represent the initial temperature of the melt, whereas the lower temperature estimates from zircon suggests that this leucogranite were initially under saturated with respect to zircon and hence the calculated temperature would not closely resemble original magmatic temperatures.

A possible magma source of the studied granitic rocks could be inferred from (Figure 7c) after Gerdes et al. [20] that shows the Homra Dom leucogranite was formed by partial melting of metagraywackes that is found in deeper part of the crust of the Arabian Nubian Shield.

Rare Earth Elements (REE_S)

The REEs content of some selected fresh leucogranite samples from G. Homra Dom are given in Table 3 and normalized to chondrite compositions using the normalized values of [21] are displayed in (Figure 6g). The analyzed samples of G. Homra Dom leucogranite have low ∑REEs (39.27-120.39 ppm) compared with the world wide granites (∑REEs 250-270 ppm) as given by [22], but ∑LREEs (32.46 – 110.23 ppm) is still higher than ∑HREEs (5.43-10.78 ppm) and ∑LREE / ∑HREE (4.96 – 13.73). That agrees with the petrographic studies, where hornblende is not detected, while zircon, allanite, apatite, titanite and monazite are the mainly accessories in G. Homra Dom leucogranite. There is a strong enrichment of the LREEs with respect to the HREEs $[(La/Yb)_N= 3.61–17.18]$ and a consistent pattern of fractionation with LREEs and HREEs groups $[(Gd/Yb)_N=0.8–2.74]$. The patterns are characterized by LREEs enrichment $[(La/Sm)_N= 2.18\text{-}5.34]$ and HREEs $[(Gd/Lu)_N=0.79\text{-}2.82]$ with marked strong negative Eu anomalies (Eu/Eu*=0.11-0.62) which indicate plagioclase fractionation. The depletion of REEs in peraluminous granites has been attributed to various processes including fractionation of monazite during partial melting of the crust, magmatic differentiation [23], hydrothermal crystallization [24] and a combination of hydrothermal leaching and magmatic differentiation.

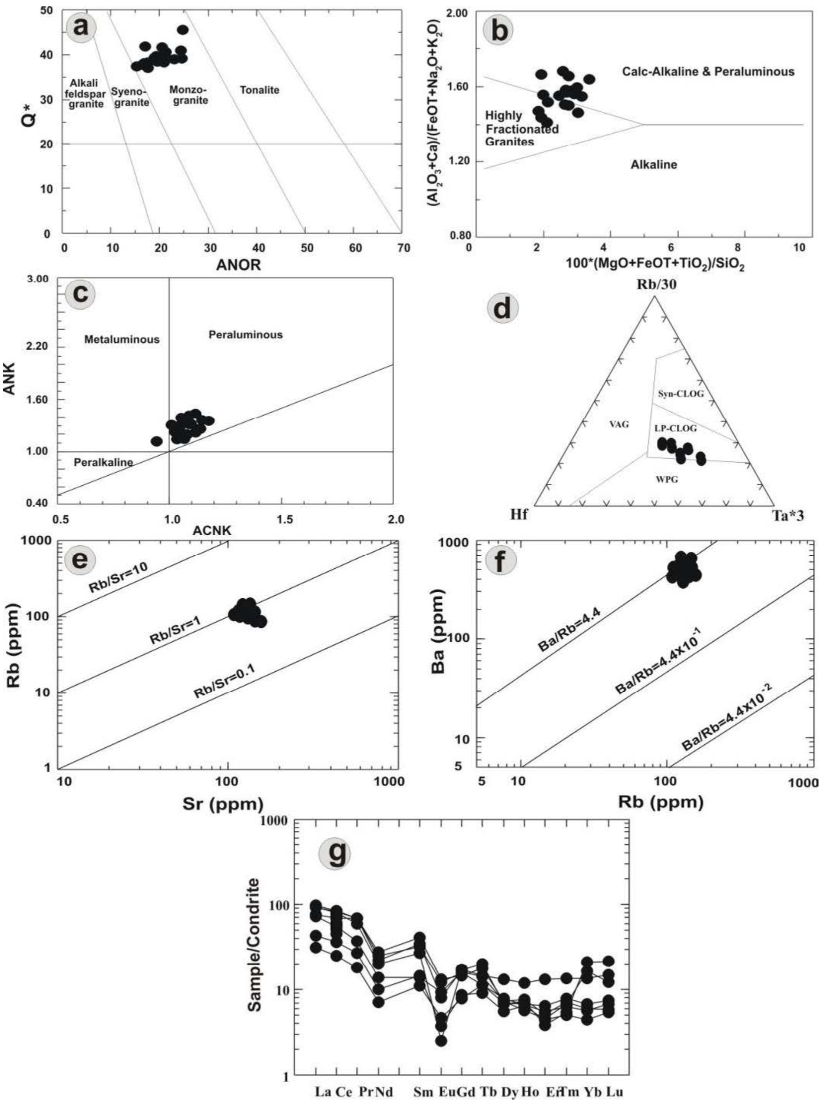

Figure 6: (a) Normative Q*- ANOR classification diagram after [11], (b) 1000 (MgO+FeO*+TiO_2)/SiO_2 versus (Al_2O_3+CaO)/(FeO*+Na_2O+K_2O) after [12], (c) Al_2O_3/Na_2O + K_2O vs. Al_2O_3/Na_2O + K_2O + CaO diagram after [13], (d) Tectonic classification (Rb/30-Hf-Ta*3) diagram after [14], (e) Rb-Sr diagram after [16], (f) Ba-Rb variation diagram, the average crustal trends after [17], (g) Chondrite-normalized REEs patterns (normalizing values after [21], G. Homra Dom, SED, Egypt.

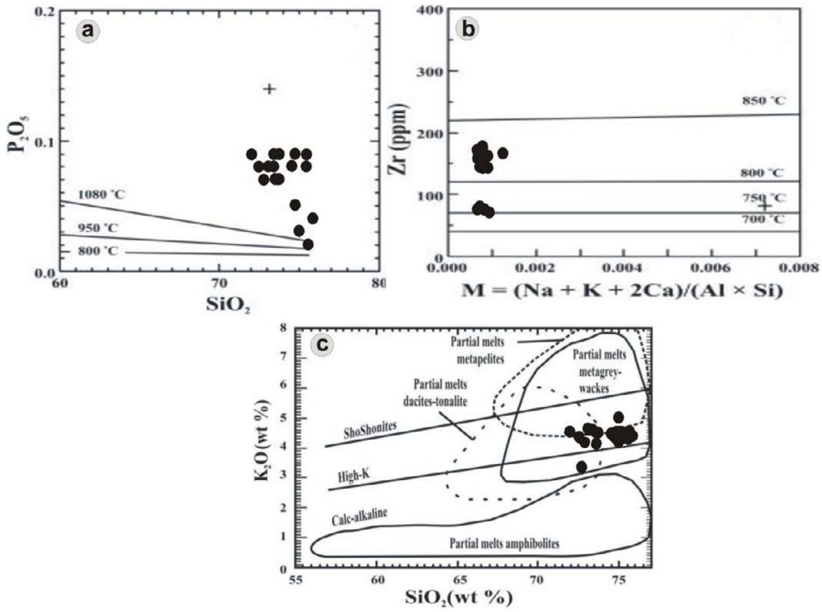

Figure 7: (a) SiO_2 *vs* P_2O_5, apatite saturation temperature estimates, (b) Zr *vs* M = (Na+K+2Ca)/(Al × Si) showing the proportion of zircon that can be dissolved in granitoid melts of various composition at different temperatures [19], (c) K_2O–SiO_2. Field of partial melts of different rock sources are after [20], G. Homra Dom, SED, Egypt.

Table 3: Rare Earth Elements (REEs) data of fresh leucogranite, G. Homra Dom, SED, Egypt.

	1	**4**	**7**	**9**	**13**	**15**	**18**	**average**
La	17.2	7.41	23.08	22.01	17.81	10.11	22.07	**17.1**
Ce	33.1	15.11	50.11	50.08	42.11	22.08	48.06	**37.24**
Pr	3.29	1.61	6.09	6.11	6.21	2.41	3.29	**4.14**
Nd	13.01	6.71	24.06	26.02	21.09	9.52	19.02	**17.06**
Sm	2.02	1.62	4.68	6.01	5.12	2.12	4.01	**3.65**
Eu	0.52	0.26	0.69	0.74	0.45	0.21	0.14	**0.43**
Gd	3.19	1.54	3.08	2.83	3.32	1.72	3.39	**2.72**
Tb	0.51	0.41	0.41	0.63	0.72	0.33	0.52	**0.5**
Dy	1.78	1.69	1.88	1.76	1.65	1.33	3.21	**1.9**
Ho	0.43	0.38	0.37	0.32	0.41	0.36	0.66	**0.42**
Er	0.82	1.07	0.89	0.72	0.61	0.71	2.07	**0.98**
Tm	0.17	0.19	0.15	0.16	0.13	0.12	0.32	**0.18**
Yb	0.97	1.09	0.93	2.71	3.42	0.73	2.22	**1.72**
Lu	0.14	0.18	0.16	0.29	0.52	0.13	0.36	**0.25**
∑ REE	77.15	39.27	116.58	120.39	103.57	51.88	109.34	**88.31**
∑ LREE	68.62	32.46	108.02	110.23	92.34	46.24	96.45	**79.19**
∑ HREE	8.01	6.55	7.87	9.42	10.78	5.43	12.75	**8.69**
∑ LREE/ ∑ HREE	8.57	4.96	13.73	11.7	8.57	8.52	7.56	**9.09**
$(La/Yb)_N$	12.28	4.71	17.18	5.62	3.61	9.59	6.88	**8.55**
$(La/Sm)_N$	5.34	2.87	3.09	2.3	2.18	2.99	3.45	**3.17**
$(Gd/Lu)_N$	2.82	1.06	2.38	1.21	0.79	1.64	1.16	**1.58**
$(Gd/Yb)_N$	2.72	1.17	2.74	0.86	0.8	1.95	1.26	**1.64**
Eu/Eu*	0.62	0.49	0.52	0.48	0.31	0.32	0.11	**0.41**
n=normalized values after [21].								

From the detailed geochemical study, it can be concluded that G. Homra Dom leucogranite originated from mostly peraluminous to metaluminous calc-alkaline magma at late-tectonic during crustal evolution at the closure of the Pan-African event [25]. In considering the petrogenesis it is suggested that the G. Homra Dom leucogranite have been mainly generated by crystal fractionation of granitic magma with additional processes at late phase crystallization (volatile- rich liquids and metasomatic effects).

Geochemistry of the sheared leucogranite

The major oxides, trace elements and CIPW norm for sheared leucogranite of G. Homra Dom area are given in Table 4. The samples of the sheared leucogranite lie between desilicification and K-metasomatism fields except two samples which lie beside the line

Table 4: Major (wt%) and trace elements (ppm) of the sheared leucogranite, G. Homra Dom, SED, Egypt.

	1	**2**	**3**	**4**	**5**	**6**	**7**	**8**	**9**	**10**	**11**	**Av.**
SiO_2	69	76.71	74.65	75.43	71.98	67.76	70.73	76.79	74.75	73.77	75.36	**73.36**
TiO_2	0.54	0.07	0.07	0.15	0.2	0.29	0.49	0.23	0.17	0.17	0.11	**0.23**
Al_2O_3	13.52	12.23	13.18	12.25	10.88	12.91	13.46	11.71	12.84	13.48	13.16	**12.69**
FeO	3.81	0.71	0.71	1.24	1.23	1.63	2.6	1.42	1.39	1.15	0.82	**1.52**
MnO	0.45	0.16	0.08	0.05	0.04	0.05	0.06	0.02	0.23	0.07	0.05	**0.11**
MgO	1.6	0.14	0.15	0.42	0.54	0.74	1.21	0.45	0.41	0.44	0.39	**0.59**
CaO	1	0.56	0.64	1.14	1.11	1.69	1.64	1.08	1.23	1.38	0.62	**1.1**
Na_2O	3.72	4.19	4.31	3.71	3.44	4.09	3.92	3.13	4.09	4.43	4.33	**3.94**
K_2O	5.87	4.3	4.95	4.39	3.22	3.86	4.27	4.72	4.35	4.75	4.83	**4.5**
P_2O_5	0.01	0.02	0.02	0.05	0.07	0.1	0.19	0.06	0.06	0.04	0.02	**0.06**
L.O.I.	0.14	0.72	1	1	7.14	6.64	1.01	0.11	0.31	0.19	0.15	**1.67**
Total	**99.66**	**99.81**	**99.76**	**99.83**	**99.85**	**99.76**	**99.58**	**99.72**	**99.83**	**99.87**	**99.84**	**99.77**
Rb	467	407	426	151	138	144	178	129	282	341	207	**261**
Sr	25	65	59	257	282	478	622	381	203	90	110	**234**
Y	122	15	15	4	9	16	9	5	13	13	14	**21**
Zr	464	69	61	102	116	160	309	187	114	121	92	**163**
Nb	72	26	24	2	8	12	9	5	16	18	9	**18**
Ba	231	162	184	646	633	1105	2426	1567	426	186	277	**713**
V	32	0	2	9	14	31	42	9	9	4	5	**14**
Cr	15	146	219	74	98	90	56	91	99	94	106	**99**
Co	4	10	9	7	7	6	1	0	0	9	6	**5**
Ni	11	7	7	5	4	5	5	4	6	5	4	**6**

FeO is total iron

separates between the Na- and K-metasomatism (Figure 8a) on K_2O-Na_2O variation diagram [26]. After the Na-metasomatism and K-metasomatism, the H^+ metasomatism (hydrolysis) is followed and characterized by formation of sericite (sericitization), which is accompanied by the release of quartz (decalcification).

Sheared leucogranite samples are plotting on AKF ternary diagram (Figure 8b) after [27] where A= Al_2O_3 - (Na_2O + K_2O), K= K_2O and F= FeO + MnO + MgO. Three samples fall in sericite facies and one sample fall in propylitic field but the other samples fall out the fields because of their high contents of Al_2O_3 and K_2O (Al_2O_3 and K_2O are related to clay minerals due to the alteration of feldspars).

The comparison of average major oxides and trace elements between the fresh and sheared leucogranite in G. Homra Dom shows that the sheared leucogranite is enriched in MgO, Na_2O and K_2O and depleted in SiO_2 and Al_2O_3. Also, they are enriched in Rb, Sr, Zr, Ba, V and Co trace elements in comparison with the average of trace elements of the fresh leucogranite (Figure 8c).

Ground Gamma Ray Spectrometry Results

In situ gamma-ray spectrometry measurements (equivalent thorium, equivalent uranium and potassium) were carried out using a portable gamma spectrometer (Model GS 256). The relation between eU and eTh-contents and eU/eTh ratios versus eU-contents among G. Homra Dom leucogranite indicate slightly positive correlation while the variation between the eU/eTh ratios and eTh-contents shows dispersive correlation suggesting enrichment of uranium relative to thorium which indicate that uranium had been added to these leucogranite (Figure 9). The relationship between eU versus eTh and eU/eTh ratio versus eTh and eU reflect strong positive relation along the sheared leucogranite (Figure 9) that means the eU/eTh ratio tends to increase with uranium mobilization and post magmatic redistribution.

Detailed spectrometric studies for the radioactive anomalies in the sheared leucogranite zone along N-S profiles at a grid 1 x 1 m were constructed. Results of the gamma-ray spectrometric survey of G. Homra Dom are illustrated in the form of contour maps (Figure 10). The eTh- and eU-maps show three zones along the sheared zone. The eU-map is close to the eTh-map which clarifies the high radioactive zones. The contour line 40 ppm eU which delineate the younger leucogranite reflects a lithological discontinuity between the country rocks and this pluton.

According to Clark et al. [28], the eU/eTh is equal about 0.33 in granitic rocks. The eU/eTh ratio mainly depends on the mobile element (uranium) so, this ratio is important for uranium-enriched areas. Enrichment in uranium will be indicated by an increase of this ratio above 0.33 in leucogranite. The leach out of uranium or initially uranium poor leucogranite will be indicated by the decreasing of this ratio to less than 0.33. This reflects an increase of thorium relative to uranium during magmatic fractionation. The overlap between the high eU/eTh and the eTh map is helpful in delineating the thorium enrichment zones within G. Homra Dom. In order to get an idea about the remobilization of uranium in G. Homra Dom which area constructing the contour map of the (eU-eTh/3.5) enables the delineation of the limit between the negative contours (leaching) and positive contours (deposition) (Figure 10a). In order to get an idea about the remobilization of uranium in the area, the expected original content of uranium is calculated by dividing eTh content by the Clark eTh/eU ratio (3-4) in granite [28]. The result is the hypothetical (original) uranium distribution [29]. It is very helpful in defining the trends of uranium migration. It forms narrow elongated zones that encountered as surrounding the sheared G. Homra Dom.

From the alternative and high positive anomalies especially that are associated with the sheared G. Homra Dom the direction of the uranium mobilization can be traced with directions trending from the negative anomalies to the high positive ones as shown in (Figure 10b). The relationship between eU with eTh and the eU with eU/eTh reflect a positive relation (Figure 10c). That means the eU/eTh ratio tends to increase with uranium mobilization and post magmatic redistribution in G. Homra Dom and this could be a favorable economic criterion into zones with G. Homra Dom.

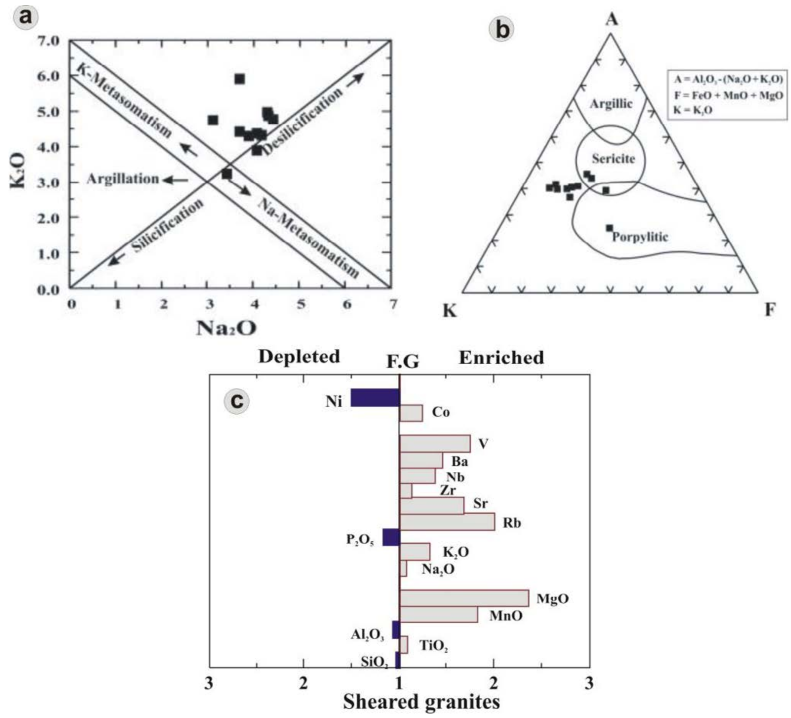

Figure 8: (a) K_2O-Na_2O variation diagram, showing the alteration type after [26], (b) AKF ternary diagram after [27], and (c) Bar diagram showing the enrichment and depletion of some major oxides and trace elements between the fresh and sheared leucogranite, G. Homra Dom, SED, Egypt.

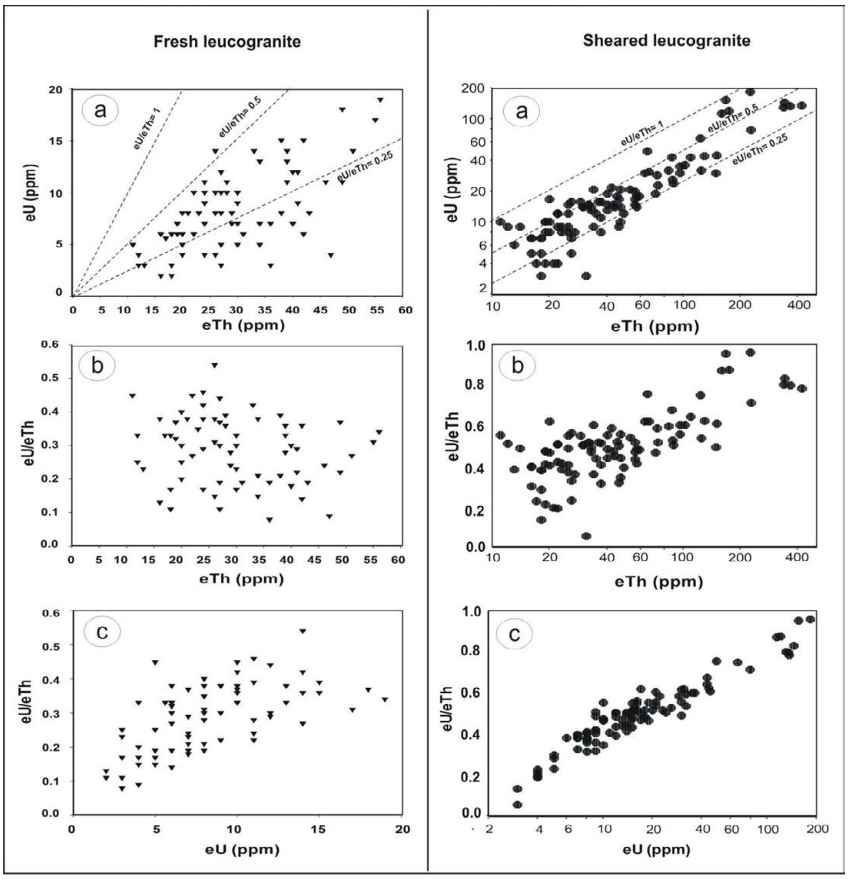

Figure 9: Binary diagrams of radioelement concentrations in fresh and sheared leucogranites, G. Homra Dom, SED, Egypt.

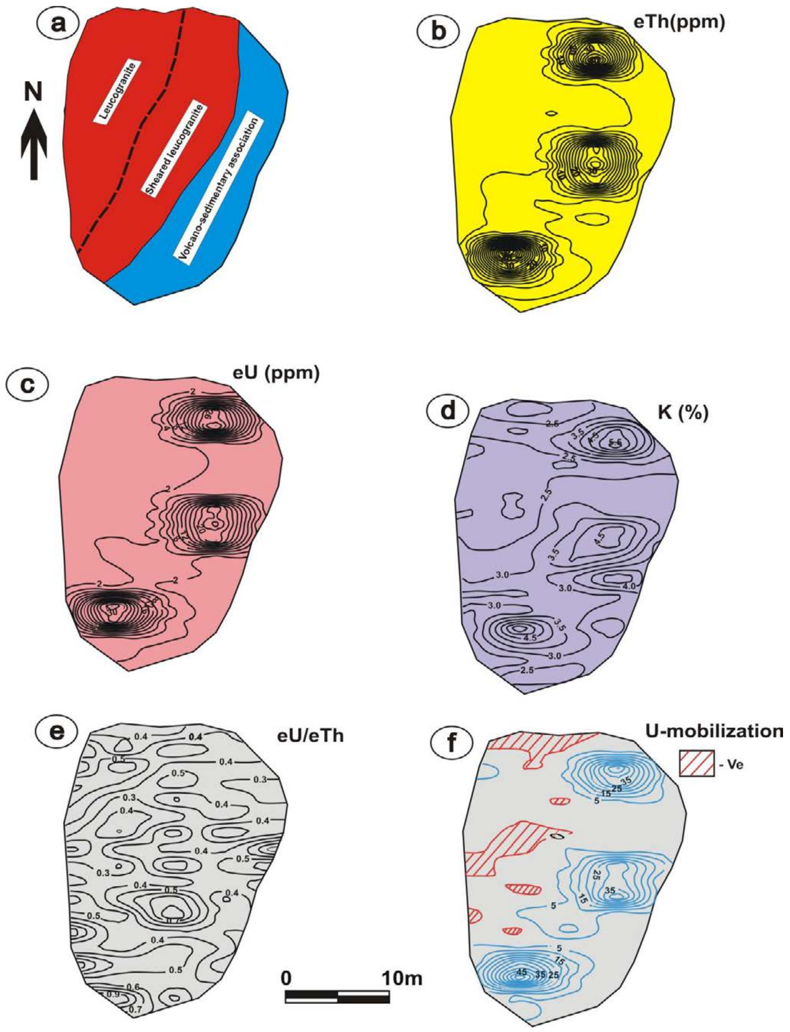

Figure 10: Simplified Geologic and contour maps of eU, eTh, K, eU/eTh and U-mobilization in sheared zone, G. Homra Dom leucogranite, SED, Egypt.

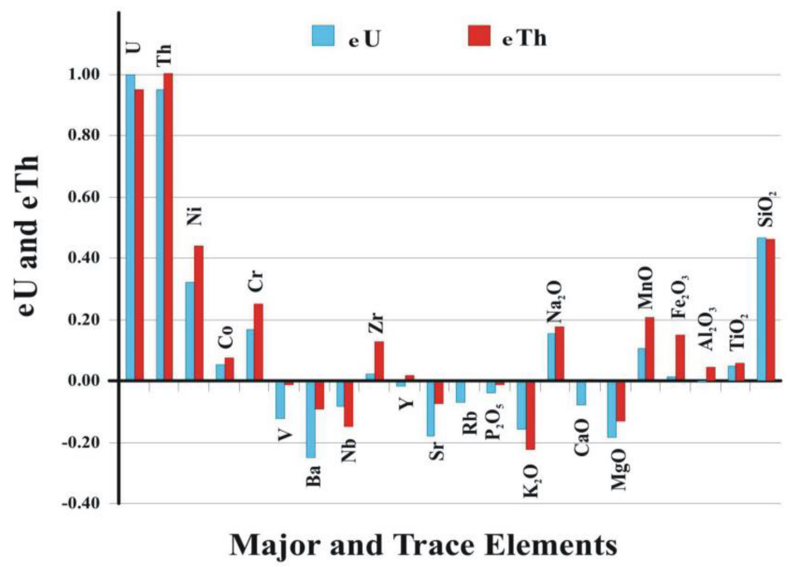

Figure 11: Bar diagram showing the correlation coefficients of some major and trace elements with eU and eTh for the G. Homra Dom leucogranite, SED, Egypt.

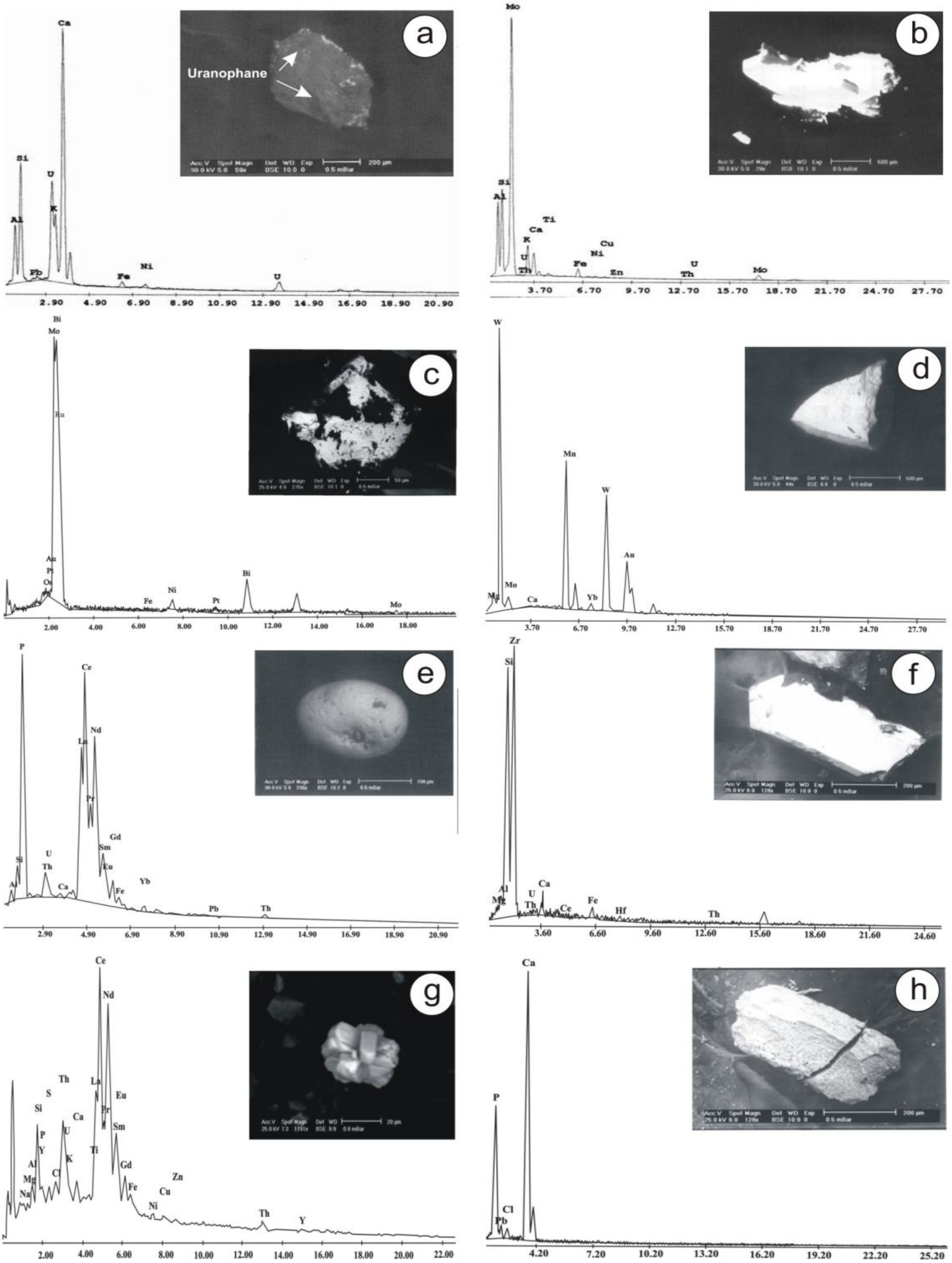

Figure 12: ESEM image and EDX spectrum for identified minerals.
(a) Uranophane (b) Molybdenite (c) Bismuth (d) Wolframite
(e) Monazite (f) Zircon (g) Allanite (h) Apatite

The correlation matrix between eU, eTh and some major and trace elements for G. Homra Dom leucogranite was calculated in order to study the interrelationships between these elements. Based on this matrix, a bar diagram is shown in (Figure 11). Both eU and eTh correlate similarly with other major and trace elements, reflecting their geochemical coherence during the crystallization of the magma. The positive correlations with major elements, SiO_2, TiO_2, MnO and Na_2O are a further indication for their magmatic evolution.

Mineralogy

Heavy mineral fractions from G. Homra Dom leucogranite (fresh and sheared) were examined by XRD and ESEM (Environmental Scanning Electron Microscope model Philips XL30) supported by a semi-quantitative energy dispersive spectrometer (EDS) unit. These analyses were carried out in the laboratories of the Nuclear Materials Authority (NMA), Cairo, Egypt. The identified minerals are confirmed by the ESEM (Figure 12).

Uranophane [$Ca(UO_2)_2(SiO_2)_2(OH)_2.5H_2O$] occurs as micro-fractures filling or coating on feldspars. Uranophane is very soft with different grades of yellow to waxy dull colour and contains 40.6% U (Figure 12a). Molybdenite [MoS_2] occurs as irregular grains and confirmed by ESEM (Figure 12b). The molybdenite contains 62.5% Mo in association with 20.36% Bi and minor amount of Ti, Ni, Zn, U and Th. Bismuth [Bi] is a native mineral with creamy white to pinkish cream and brownish tarnishes. It is confirmed by ESEM (Figure 12c) the analyses indicate up to 69.8% Bi associated 5.2% Mo.

Wolframite [$MnWO_4$] is brownish black colour and mainly composed of 60.6% W with 9.1% Mn and 9.2% Fe and confirmed by ESEM (Figure 12d). The wolframite occurs as accessory mineral in leucogranite, as well as hydrothermal origin [30]. Monazite [(Ce,La,Nd,Th) (PO_4,SiO_4)] is considered as LREE-bearing minerals, especially Ce and confirmed by ESEM (Figure 12e). Zircon [Zr (SiO_4)] is confirmed by the ESEM analysis (Figure 12f) and contains 59.7% Zr, 6.8% Th, 3.5% Hf and 1.5% U.

Allanite [$(Ce,Ca,Y,Th)_2$ $(Al,Fe,Mg)_3$ Si_3 O_{12} (OH)] occurs as prismatic crystals of brown to brownish black colour and confirmed by ESEM (Figure 12g) and contains 33.6% Ce, 16.3% La, 12.4% Nd, 11.9% Th, 3.7% Pr, 3.1% U and 2.4% Y. Apatite [$Ca_5(PO_4)_3$(OH, F, Cl)] is contains 65.16 % Ca, 25.77 % P, 6.87 % Pb and 2.21 % Cl and confirmed by ESEM (Figure 12h).

The identified minerals from the sheared leucogranite are formed at the end of the magmatic stage of G. Homra Dom leucogranite. The residual magmatic solution enriched by mineralizing fluids containing (Bi, W, Sn, Mo, F, Th and U) rises as postmagmatic hydrothermal episode along the southern and eastern contacts with the volcano-sedimentary association. The presence of fluorite accompanying this mineralization indicates that the alteration process is mainly due to hydrothermal activity.

Discussion

G. Homra Dom leucogranite is elongated shape trending NWW-SSE and bounded by two major sinstral strike slip faults (NNW-SSE trend), which act as channels for crustal and mantle-derived magmas [31,32] as well as pass way for hydrothermal fluids [33,34]. Major strike-slip faults initiate deep within the crust and the lithospheric mantle due to rheological weakening [35]. During the exhumation of these tectonic systems, the ascent of magmas as well as hot lower crustal, and magmatic - derived fluids is followed by the downward flow of cold surface-derived water. The leucogranite magma intrudes the country rocks (amphibolite, metavolcanic and volcano-sedimentary association) with sharp contacts and classified as monzogranite.

Among U-rich peraluminous leucogranite represent an ideal source for the formation of U-deposits because most of their uranium is hosted in easily leachable [36]. The most pronounced hydrothermal alterations in G. Homra Dom leucogranite is expressed as the albitization and sericitization of feldspars, muscovitization of biotite and hematitization along the eastern and the southern parts of G. Homra Dom leucogranite. The metasomatism of the magmatic stage is connected with fluids emanating from a liquid magma body and metasomatizing the solid host rocks while the metasomatic processes of the post magmatic stage are retrogressive and are connected with hydrothermal solutions both emanating from the cooling magma and/or other heated exogenic sources, due for instance to the mixing of juvenile water with meteoric water [37].

At the end of magmatic stage which formed G. Homra Dom leucogranite, the magmatic solution enriched by mineralizing fluids containing (Bi, W, Sn, Mo, F, Th and U) it rises as post magmatic hydrothermal episode along the south eastern contact, forming hematitized and sheared leucogranite zone enriched by the tungsten-bismuth-molybdenum association and fluorite. G. Homra Dom leucogranite exhibits calc-alkaline affinity and peraluminous to met aluminous compositions. Based on the petrological and geochemical features, G. Homra Dom leucogranite could be generated by fractional crystallization of granitic magma in late- to post collision. The low average of the REEs (∑88 ppm) in the studied leucogranite is below the average of the world wide leucogranite (∑250-270 ppm) as given by [22].

Uranium mineralization represented by gummite (altered uraninite) inclusions in feldspars points to magmatic type [38]. However, presence of secondary metamict allanite, zircon and uranophane firmly indicate release of uranium during later alterations. Clouding of feldspars points to the metasomatic alterations and the sericitisation and sassuritization which indicate low temperature alterations in leucogranite [39]. Major oxide composition exhibits Na-enrichment in mineralized leucogranite (Na_2O: 3.13% - 4.133%) and K-enrichment in non-mineralized leucogranite (Na_2O: 3.29% - 34.54%). Wide variation in U/Th ratio also supports the prevalence of both magmatic and later alteration in the leucogranite.

Conclusion

We can conclude that the G. Homra Dom leucogranite was formed through the implacement of calc-alkaline magma of peraluminous to met aluminous in nature under a compressional regime. Crystal fractionation of this magma, as evidenced from the use of REEs and trace elements, dominated by separation of plagioclase and alkali-feldspars with minor mafic minerals (biotite) led to the crystallization of G. Homra Dom leucogranite pluton, Additional processes such as hydrothermal and sub solidus metasomatism affected these leucogranite leading to the mobilization of REE and crystallization of different mineralization.

The relationship between eU versus eTh and eU/eTh ratio versus eTh and eU reflect strong positive relation along sheared leucogranite that means the eU/eTh ratio tends to increase with uranium mobilization and post magmatic redistribution. Uranium is leached during hydrothermal activity or during circulation of groundwater from certain minerals such as monazite, allanite and epidote. The uranium is brought into solution by acidic conditions and is deposited when this acidity is neutralized so it recorded found coating the feldspars and fracture filling.

Acknowledgements

The authors wish to thanks the late Prof. Dr. M.E. Ibrahim and Prof. Dr. H.M. Shalaby, Nuclear Materials Authority, for interest as well as for help during field work, critical comments and for guidance during the progress of the manuscript.

References

1. El Gaby S, List FK, Tehrani R (1988) Geology evolution and metallogenesis of the pan african belt in Egypt. In: El Gaby S, and Greiling RO, Eds., The Pan African Belt of Northeast Africa and Adjacent Aeas, Viewing, Berlin. 17-70.
2. Johnson PR, Andresen A, Collins AS, Fowler AR, Fritz H, et al. (2011) Late Cryogenian-Ediacaran history of the Arabian–Nubian Shield: A review of depositional, plutonic, structural, and tectonic events in the closing stages of the northern East African Orogen. J African Earth Sci 61: 167-232.
3. Lundmark AM, Andresen A, Hassan MA, Augland LE, Boghdady GY (2012) Repeated magmatic pulses in the East African Orogen in the Eastern Desert, Egypt: An old idea supported by new evidence. Gondwana Res 22: 227-237.
4. Abdel Rahman, AFM, Martin RF (1990) The Mount Gharib A-type granite Nubian Shield: role of metasomatism at the source. Contrib Mineral Petrol 104: 173-183.
5. Moghazi AM, Hassanen M A, Hashad M H, Mohamed F H (2001) Garnet-bearing leucogranite in the El-Hudi area, southern Egypt: evidence of crustal anatexis during Pan-African low pressure regional metamorphism. J Afr Earth Sci 33: 245-259.
6. Moghazi AM, Hassanen MA, Mohamed FH, Ali S (2004) Late Neoproterozoic strongly peraluminous leucogranites, South Eastern Desert, Egypt: petrogenesis and geodynamic significance. Contrib Mineral Petrol 81: 19–41.
7. Assaf HSA, Ibrahim ME, Rashed MA (1997) Geologic and Radiometric Studies for Shalatin - Halaib Radioactive Mineral Occurrences, South Eastern Desert, Egypt. Int Res J Geol Min 6: 38-52.
8. Streckeisen A (1976) To each plutonic rock its proper name. Earth Sci 12: 1-33.
9. Padfield T, Grey A (1971) Major element rock analyses by X-ray fluorescence-a simple fusion method. Philips Bull, Analytical Equipment 35.
10. Shapiro L, Brannock WW (1962) Rapid analysis of silicate, carbonate and phosphate rocks. Contributions to Geochemistry 1144a: 56.
11. Streckeisen AL, Le Maitre, RW (1979) A chemical approximation to the QAPF classification of the igneous rocks. News Jarb Mineral, Abhanddlungen 136: 169-206.
12. Sylvester PJ (1989) Post-collision alkaline granites. J Geol 97: 261-280.
13. Maniar PD, Piccoli PM (1989) Tectonic discrimination of granitoids. Geol Soc Am Bull 101:635-643.
14. Pearce JA, Harris NB, Tindle AG (1984) Trace element discrimination diagrams for the tectonic interpretation of granitic rocks. J Petrol 25: 956 - 983.
15. Nockolds SR, Allen R (1952) The geochemistry of some igneous rock series. Geochim & Cosmochim Acta 4: 105-142.
16. Hanson GN (1978) The application of trace elements to the petrogenesis of igneous rocks of granitic composition, Earth Planet Sci Lett 38: 26-43.
17. Taylor SR (1965) The application of trace elements data to problems in petrology. phys and chem of the earth, Pergamon Press Oxford 6: 1-133.
18. Beus AA, Grigorian SV (1977) Geochemical exploration methods for mineral deposits. Nedra, Moscow, 287.
19. Watson E, Harrison TM (1983) Zircon saturation revisited: temperature and composition effects in a variety of crustal magma types. J Earth Planet Sci Lett 64:295-304.
20. Gerdes A, Worner G, Henk A (2000) Post collisional granite generation and HT – LP metamorphism by radiogenic heating: the Variscan South Bohemian Batholith. J of the Geol Society of London. 157:577-587.
21. Anders E, Grevesse N (1989) Abundances of the elements: Meteoritic and Solar. Geochimica et Cosmochimica Acta 53: 197-214.
22. Wedepohl KH (1969) Yttrium and lanthanides:Handbook of Geochemistry, Springer, New York 106:442.
23. Cuney M, Friedrich M (1987) Physicochemical and crystal –chemical controls on accessory mineral paragenesis in granitoids: Implications for uranium metallogenesis, Bull Mineral 110: 235-247.
24. Cocherie A, Rossi Ph, LeBel L (1984) The variscan calc-alkaline plutonium of western Corsica: mineralogy and major and trace element geochemistry. Phys Earth Plant Inter 35: 145-178.
25. Harris NBW (1983) Alkaline complexes from the Arabian Shield. J Afr Earth Sci 3: 83-88.
26. Cuney M, Leroy J, Volivezo PA, Daziano C, Gambda M, et al. (1989) Metallogenesis of the uranium mineralized Achala granitic complex, Argentina: comparison with Hercynian peraluminous leucogranites of Western Europe. Vienna IAEA 20: 211-232.
27. Meyer C, Hemley JJ (1967) Wall rock alterations. Geochemistry of hydrothermal ore deposits (H. G. Barnes, ed.), Winston Inc. New York. 670.
28. Clark SPJ, Peterman ZE, Heier KS (1966) Abundances in uranium, thorium and potassium. In: Handbook of physical contents, Geol Soc Am 97: 521-541.
29. Cambon R (1999) Uranium resource development in the Eastern Desert of Egypt; Mapping and prospecting in granitic formation. IAEA/RU 61.
30. Berry LGM, Mason B, Dietrich RV (2000) Mineralogy. CBS Publishers and Distributors, New Delhi, India. 561.
31. Brown M (2010) The spatial and temporal patterning of the deep crust and implications for the process of melt extraction. Philos T Roy Soc 368: 11-51.
32. Pirajno F (2010) Intracontinental strike-slip faults, associated magmatism, mineral systems and mantle dynamics: examples from NW China and Altay-Sayan (Siberia). J Geodyn 50: 325-346.
33. Faulkner DR, Jackson CAL, Lunn RJ, Schlische RW, Shipton ZK et al. (2010) A review of recent developments concerning the structure, mechanics and fluid flow properties of fault zones. J Structural Geol 32: 1557-1575.
34. Lopez Moro FJ, Moro MC, Timon SM, Cembranos ML, Cozar J (2012) Constraints regarding gold deposition in episyenites: the Permian episyenites associated with the Villalcampo Shear Zone, central western Spain. Int J Earth Sci 102: 721-744.
35. Cao S, Neubauer F (2016) Deep crustal expressions of exhumed strikeslip fault systems: shear zone initiation on rheological boundaries. Earth Sci Rev 162:155-176.
36. Cuney M (2014) Felsic magmatism and uranium deposits. Bull Soc Geol Fr 185:75-92.
37. Korzhinskii DS (1953) Outline of metasomatic processes. In: Main problems on the science of magmatogenic ore deposits. Acad Sci Publishing, Moscow. (In Russian) German edition, 1965. Abriss der metasomatischen Prozesse, Akad Verl Berlin 334-456.
38. Frondel C (1958) Systematic mineralogy of Uranium and Thorium.1064: 400.
39. Morad S, El-Ghali MAK, Caja MA, Sirat M, Al-Ramadan K, et al. (2009) Hydrothermal alteration of plagioclase in granitic rocks from Proterozoic basement of SE Sweden. Geol J 45: 105-116.